Hot Electron Temperature and Coupling Efficiency Scaling with Prepulse for Cone-Guided Fast Ignition

T. Ma,[1,2] H. Sawada,[2] P. K. Patel,[1] C. D. Chen,[1] L. Divol,[1] D. P. Higginson,[1,2] A. J. Kemp,[1] M. H. Key,[1] D. J. Larson,[1] S. Le Pape,[1] A. Link,[1,3] A. G. MacPhee,[1] H. S. McLean,[1] Y. Ping,[1] R. B. Stephens,[4] S. C. Wilks,[1] and F. N. Beg[2]

[1]*Lawrence Livermore National Laboratory, Livermore, California 94550, USA*
[2]*University of California-San Diego, La Jolla, California 92093, USA*
[3]*The Ohio State University, Columbus, Ohio 43210, USA*
[4]*General Atomics, San Diego, California 92186, USA*
(Received 3 December 2011; published 16 March 2012)

The effect of increasing prepulse energy levels on the energy spectrum and coupling into forward-going electrons is evaluated in a cone-guided fast-ignition relevant geometry using cone-wire targets irradiated with a high intensity (10^{20} W/cm^2) laser pulse. Hot electron temperature and flux are inferred from $K\alpha$ images and yields using hybrid particle-in-cell simulations. A two-temperature distribution of hot electrons was required to fit the full profile, with the ratio of energy in a higher energy (MeV) component increasing with a larger prepulse. As prepulse energies were increased from 8 mJ to 1 J, overall coupling from laser to all hot electrons entering the wire was found to fall from 8.4% to 2.5% while coupling into only the 1–3 MeV electrons dropped from 0.57% to 0.03%.

DOI: 10.1103/PhysRevLett.108.115004 PACS numbers: 52.50.Jm, 52.38.Kd, 52.38.Mf, 52.70.La

Fast Ignition (FI) [1,2] is an approach to inertial confinement fusion (ICF), in which a precompressed deuterium-tritium fuel is rapidly driven to ignition by an external heat source. This scheme can ignite lower density fuel leading, in principle, to higher gains than possible with conventional ignition. In the reentrant cone approach to FI, a hollow cone is embedded in the fuel capsule to provide an open evacuated path free of coronal plasma for an intense laser beam to generate a flux of energetic electrons at the tip of the cone which can then propagate to the compressed fuel core. However, the presence of preformed plasma in the cone, arising from the inherent laser prepulse which ablates the inner cone wall, can strongly affect the spatial, energy-spectral, and angular characteristics of these laser-generated hot electrons and thus the efficiency with which their energy can be coupled to the core.

Previous works by Baton *et al.* [3] and Van Woerkom *et al.* [4] showed that significant prepulse could have a detrimental effect on coupling beyond the cone tip. MacPhee *et al.* [5] demonstrated that even a small prepulse could result in significant filamentation of the laser beam in the preplasma, limiting the penetration of the laser, and accelerating energetic electrons transversely. These results were achieved using either imaging of $K\alpha$ x-ray emission from the cone target itself or measuring the intensity of the $K\alpha$ spot in a region beyond the cone tip. However, while these techniques provided a spatial distribution of $K\alpha$ in various areas of the interaction, no spectral information regarding the electron flux could be inferred. Comparisons of preplasma versus no preplasma conditions by Baton *et al.* were achieved by doubling the fundamental laser frequency to create a high contrast. This provided a clean interaction surface for the main laser, but complicated the comparison, as the absorption mechanisms would be different for the very different $I\lambda^2$. In the MacPhee *et al.* study, electrons were electrostatically confined within the isolated cone target. The significant amount of recirculation of the hot electrons within the cone walls and plasma allows only limited conclusion of the electron source at the cone tip in either the experiment or simulations.

In this Letter, we present the first quantitative scaling of coupling as a function of prepulse in an intense laser-cone interaction. Through the use of cone-wire targets [6], we demonstrate the existence of a two-temperature hot electron distribution within the target and characterize its flux and energy spectrum entering a 40 μm diameter wire at the cone tip, and correlate these quantities with the amount of preformed plasma in the cone.

The experiment was performed on the Titan laser at LLNL, of $\lambda_0 = 1.054$ μm wavelength, 150 ± 10 J, focused to an 8 μm full width at half maximum (FWHM) focal spot in a 0.7 ± 0.2 ps pulse length. The intrinsic prepulse of the laser was measured at 8 ± 3 mJ in a 1.7 ns duration pulse prior to the main beam. Varying prepulse levels, up to 1 J, were produced by injecting an auxiliary nanosecond-duration laser colinear with the main short pulse laser. This auxiliary laser had a similar focal spot distribution as the main beam and was timed to overlap the intrinsic prepulse.

The target, shown in Fig. 1, was a 1 mm long Au hollow cone with 30° full opening angle, 20 μm wall thickness, 30 μm internal tip diameter, and 11 μm tip thickness. A 1.5 mm long, 40 μm diameter Cu wire was glued to the outer cone tip. The wire diameter is chosen to match the nominal 40 μm optimum ignition hot spot diameter in a FI target [7], and its quasi 1D geometry allows for single shot

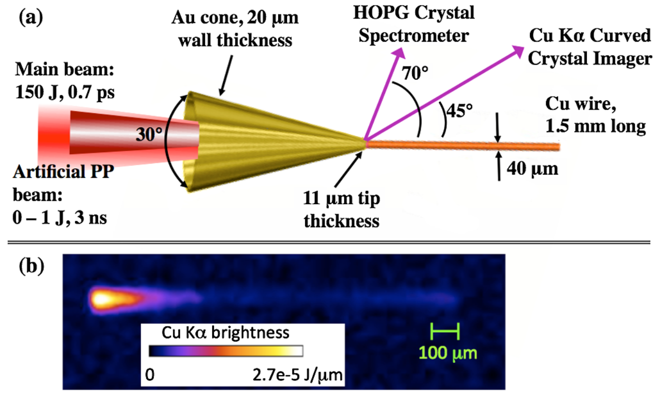

FIG. 1 (color online). (a) Schematic of the cone-wire target and diagnostic geometry. (b) Example of the 2D spatially resolved image of $K\alpha$ emission along the wire.

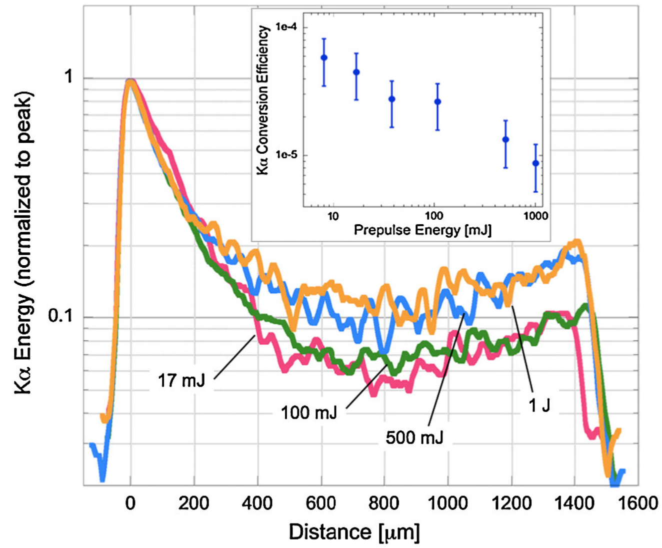

FIG. 2 (color online). Transversely integrated lineouts along the Cu wire from the $K\alpha$ imager for 17 mJ of prepulse (pink), 100 mJ (green), 500 mJ (blue), and 1 J (orange). All profiles are normalized to their peak. (inset) Total $K\alpha$ conversion efficiencies in the wire as a function of prepulse. The statistical shot-to-shot variation, as well as the systematic error in the absolute $K\alpha$ yield were added in quadrature to provide the $\sim \pm 40\%$ error bars applied to all points.

characterization of the electron energy deposition as a function of depth without the complexity of a diverging electron beam [6,8]. Both the main laser pulse and the artificial prepulse beams were focused to the inner cone tip surface.

Hot electron-induced $K\alpha$ emission from the Cu wire was measured with a spherically bent quartz crystal imager [9], providing 2D spatially resolved images of the Cu $K\alpha$ radiation within a ~6 eV bandwidth centered at 8.048 keV. An absolutely calibrated highly oriented pyrolitic graphite (HOPG) spectrometer [10] provided an absolute brightness of the total Cu $K\alpha$ emitted from the wire. Because of its narrow bandwidth, the imager response is sensitive to the ionization of the Cu material as it heats up [11]. However, a linear scaling between the integrated $K\alpha$ signal measured on the imager versus the integrated line emission from the spectrometer for this data indicated this was a negligible effect in this experiment.

A series of shots were taken with prepulse energies of 8 ± 3 mJ (intrinsic), 17 ± 3 mJ, 30 ± 10 mJ, 100 ± 10 mJ, 500 ± 10 mJ, and 1000 ± 10 mJ. Transversely integrated $K\alpha$ lineouts along the wire axis, taken from the 2D imager, were corrected for view angle and opacity and converted to units of J/μm of $K\alpha$ photons by cross-calibration against the absolute $K\alpha$ yield measured with the spectrometer [6,8]. The coupling efficiency from laser energy to $K\alpha$ is plotted in Fig. 2 along with the spatial $K\alpha$ profiles normalized to their peak values. The $K\alpha$ coupling efficiency is observed to fall with increasing prepulse over the entire range of measurements, with a $7\times$ total reduction between 8 and 1000 mJ. The spatial lineouts for the different shots share qualitatively similar features: the signal falls off quasiexponentially over the first 500 μm of the wire, levels off in the center, and rises again in the final ~400 μm to form a peak at the end of the wire. However, the relative signal between the beginning and end of the wire changes with prepulse level—the higher prepulse shots showing relatively stronger emission further into the wire.

The particle-in-cell code LSP [12] was used to model the hot electron propagation and $K\alpha$ generation in the wire target. LSP employs a direct implicit particle push, allowing solid density and cold plasmas to be modeled at both large scales and long times. Collisions between the background fluid particles of the wire are handled using LMD [13,14] collision frequencies, while injected hot electrons use a test particle collision model from [15]. The Cu wire was modeled in 2D R-Z geometry at a full spatial scale of 20 μm radius and 1.5 mm length, with a 1 μm cell size. It was surrounded at the end and sides by a 500 μm vacuum region, with an additional 500 μm of material placed behind the injection plane to absorb rear-going particles. The Cu equation of state including ionization was described using the PROPACEOS model [16]. $K\alpha$ production was modeled using the Hombourger model [17]. Other x-ray emission processes were calculated using the Integrated Tiger Series (ITS) Xgen tables [18].

A beam of kinetic electrons was injected uniformly over the cross-section of the wire, along the wire axis, in a 0.7 ps FWHM gaussian temporal pulse. The initial energy spectrum of the injected electrons was described by either a one- or two-temperature relativistic Maxwellian of the form $dN/dE \sim \gamma\sqrt{(\gamma^2 - 1)}\exp(-E/kT)$, where γ is the relativistic factor. Initial divergence angle of the injected electron beam was found to have only a relatively small effect. Simulations were typically run to 20 ps to provide time for complete relaxation of the hot electron distribution. The input parameters varied included the hot electron temperatures, T_{hot1} and T_{hot2}, the total electron energy, and the number fraction, R, of electrons in the T_{hot2} component (where $T_{\mathrm{hot2}} > T_{\mathrm{hot1}}$). A large set of simulations was performed with T_{hot1} and T_{hot2} varied from 0.1 to 10 MeV, R from 0 to 0.02, and the total injected electron energy, E_{tot}, from 1 to 30 J. The simulated $K\alpha$ profiles were convolved with a 25 μm instrumental resolution and compared with the data. The best fit for each shot was found by concurrently matching the peak $K\alpha$ and exponential slope at the front of the wire, the rise at the end of the wire, and the total $K\alpha$ integrated over the full profile.

Single-temperature electron distributions were found not to reproduce the measured profiles. Figure 3(a) shows two examples of fits of single-temperature distributions to a shot with low (17 mJ) prepulse. The peak value and slope of the first third of the wire is sensitive to both temperature and total energy and can be well fit with a single several hundred keV temperature electron distribution. However, the emission over the latter two-thirds of the wire is underestimated. This part of the wire requires a higher temperature in the MeV range. Two-temperature distributions are able to fit the data over the entire profile. Figure 3(a) also shows the best fit for the same shot where now $T_{\mathrm{hot1}} =$ 300 keV with $E_{\mathrm{tot1}} = 1.99$ J, and $T_{\mathrm{hot2}} = 7$ MeV with $E_{\mathrm{tot2}} = 8.61$ J. The total injected energy of 10.6 J corresponds to a coupling efficiency of 7.1% of laser energy to hot electrons exiting the cone tip and entering the wire. The fitting procedure shows that the low temperature component, T_{hot1}, can be matched to ± 50 eV. The high temperature component, T_{hot2}, however, cannot be derived accurately from the $K\alpha$ profile alone. An additional constraint, the energy spectrum of electrons in vacuum measured along the wire axis [19,20] is employed. The slope temperature of the escaped electron spectrum, which has been shown to correspond well to the original high energy portion of the electron distribution at the source [21], was used to bound the T_{hot2} in the simulation to between 4 and 8 MeV.

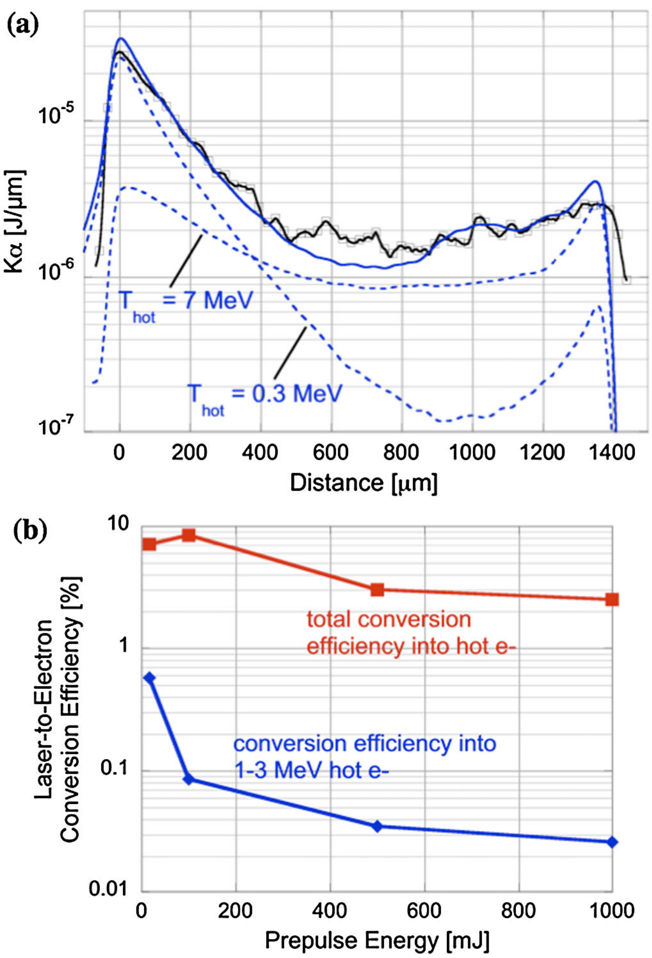

FIG. 3 (color online). (a) Single-temperature distribution fits (dotted) cannot fully capture the pattern of $K\alpha$ emission along the 1.5 mm long wire. A two-temperature electron distribution (solid) is required to fit the experimental profile (solid, bold). (b) The inferred overall laser-to-electron and laser-to-1–3 MeV electron conversion efficiency over prepulse energies ranging from 10–1000 mJ.

The overall laser-to-electron coupling efficiency falls from 7.1% to 2.5% between the lowest and highest prepulse cases. This reduction is mirrored by each component of the electron distribution, but with the relative fraction of the energy going into the hotter component increasing with increasing prepulse. At higher prepulse levels, nearly all electrons captured into the wire belong to the higher T_{hot2} component. From this analysis, the conversion efficiency into the 1–3 MeV electrons most relevant for FI could also be extracted out of the overall electron distribution. (The 1–3 MeV electrons represent those which most efficiently deposit energy within the hot spot, with higher energy electrons depositing correspondingly less.) As shown in Fig. 3(b), in the case of the lowest 10 mJ prepulse, the coupling into 1–3 MeV electrons was found to be below 1%. Further increasing the prepulse energy only magnifies the effect on conversion efficiency into the 1–3 MeV electrons, dropping its coupling by a factor of 22 between the smallest and largest prepulses, while overall conversion efficiency from laser to hot electrons falls just a factor of 3 over the same prepulse range.

Table I summarizes the results of the best fit distributions for each of the four profiles shown in Fig. 2. Regardless of prepulse energy, the overall conversion efficiency of laser into hot electron energy in the wire is dominated by the hotter temperature component (1.3% for $T_{\mathrm{hot1}} = 300$ keV vs 5.7% for $T_{\mathrm{hot2}} = 7$ MeV for the lowest prepulse case). The estimated bounds on each T_{hot} component results in an error bar of $\pm 25\%$ on the total injected electron energy.

The characteristic rise in $K\alpha$ seen at the end of the wire can be understood by examining details of the electron motion. The bulk of the electrons travel through the wire subject to energy loss and scattering through collisions and

TABLE I. Summary of results from LSP fits to the $K\alpha$ emission profiles corresponding to 17, 100, 500, and 1000 mJ prepulse.

Prepulse energy [mJ]	E_{hot1} @ T_{hot1}	E_{hot2} @ T_{hot2}	Total laser to hot electron conv. eff	Conv. eff into 1–3 MeV *e*-
17	1.99 J @ 300 keV	8.61 J @ 7 MeV	7.1%	0.57%
100	0.74 J @ 200 keV	11.86 J @ 8 MeV	8.4%	0.09%
500	0.18 J @ 150 keV	4.32 J @ 4 MeV	3.0%	0.04%
1000	0.05 J @ 100 keV	3.75 J @ 4 MeV	2.5%	0.03%

a resistive Ohmic field. Early in time, electrons exiting the side of the wire into vacuum set up a Debye sheath with a radial electric field, $\mathbf{E_r}$. An azimuthal **B** field develops due to background current flow along the inside edge of the wire [8,22]. The forces due to these fields act in opposition and guide a population of electrons along the outside wire edge. To illustrate, Fig. 4(a) plots the trajectory of a 2 MeV test particle trapped in these fields, and also the hot electron number density at 6 ps, at which time the main electron bunch has just reached the end of the wire. On reaching the end of the wire the electron is reflected by the $\mathbf{E_z}$ sheath field and directed back into the wire by the $\mathbf{B}_\theta$ field, which has now changed polarity, as shown in Fig. 4(b) which plots the $\mathbf{E_r}$ and $\mathbf{B}_\theta$ at 4.5 and 7.0 ps. This conversion of the electron momentum from the axial to radial direction results in significantly enhanced energy loss and hence $K\alpha$ production at the end of the wire, relative to simple reflection back along the wire axis.

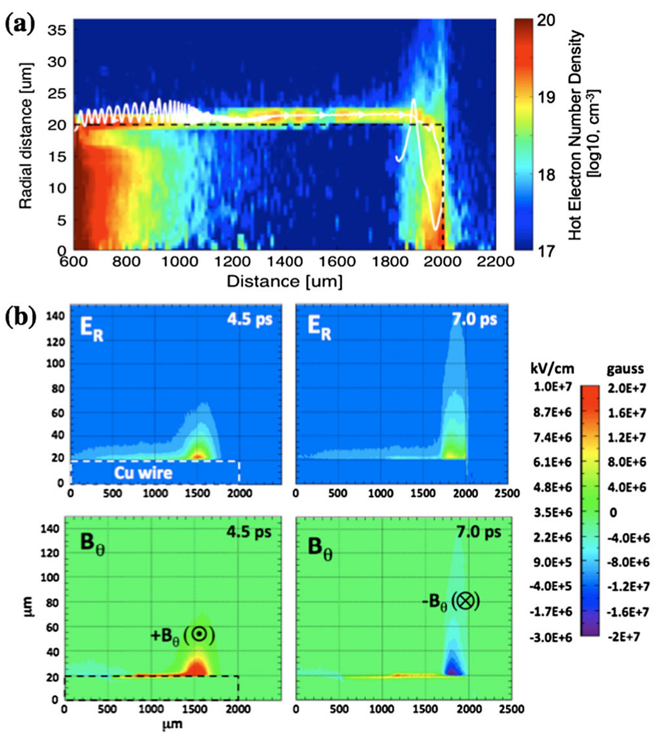

FIG. 4 (color online). (a) Hot electron number density contour at 6 ps. The trajectory of a 2 MeV test particle injected at the wire edge ($z = 600$, $r = 19$ um) is shown up to 6 ps with the white line. The electron is seen to surf along the wire and is turned at the rear surface by the $\mathbf{E_z}$ and $\mathbf{B}_\theta$ fields. (b) Radial **E** and azimuthal **B** fields before and after the electron bunch has reached the end of the wire.

2D radiation-hydrodynamics simulations of the preformed plasma were performed with the HYDRA code [23] using the measured temporal and spatial laser prepulse profiles. They show that the relativistic critical density surface moves from a distance of 20 μm from the inner surface of the cone tip with an intrinsic prepulse to 250 μm with a 1 J prepulse. The reduction in both the temperature and coupling efficiency of the T_{hot1} component is attributed to this movement of the interaction surface away from the cone tip. The laser intensity at the critical density is lower and the solid angle to the 40 μm diameter wire is reduced. In contrast, the increased fraction of the T_{hot2} component may be an indication of two effects: (i) an increased relative generation efficiency of these high energy electrons in the laser-plasma interaction (LPI) region due to the larger extent of preplasma, and (ii) the high energy electrons having a lower divergence and thus the increased distance of the LPI region from the cone tip having less influence on their coupling to the wire.

We have previously studied the full LPI in reduced scale cone-wire targets using a hybrid-PIC code [24]. These simulations predicted a multitemperature electron distribution in the wire, as well as a diminished fraction of hot electrons captured into the wire with large amounts of preplasma. Under realistic laser irradiation and intrinsic preplasma conditions, it was found that a few percent of the laser energy was coupled into several hundred keV electrons, and a slightly larger percentage into electrons with energies in the 7 MeV range. Further, a strong electrostatic sheath was seen to build up around the target, confining electrons to the wire. The results shown here are fully consistent with these simulation predictions.

In conclusion, we have presented information on the flux and energy spectrum of hot electrons as a function of prepulse level using cone-wire targets. The laser, preplasma parameters, and cone target geometry have direct relevance to the cone-guided fast-ignition scheme. The range of injected prepulse levels studied here are likely to be comparable to the intrinsic level of a full-scale FI laser, which will have much higher energy and longer pulse length. It must be emphasized that the measurements are not the total laser-to-electron conversion efficiency, but the efficiency of electrons that exit from the cone tip and could potentially contribute to the ignition of a precompressed hot spot. There will be differences in electron injection efficiency in an integrated FI target. As noted above, electrons could only escape from these cones through the wire on their tips. In a real FI target, blow-off plasma surrounding the cone will allow electrons to also escape through the cone side walls. Fits to the data using the LSP code show that a single-temperature distribution of hot electrons is not adequate to replicate the emission profile in the wire, but a two-temperature distribution with 100–300 keV and 4–7 MeV components captures the overall pattern. We have shown here that the total coupling into forward-going hot electrons, and most notably, those with energies in the 1–3 MeV range, drops steeply with increasing prepulse. This points to the necessity to minimize prepulse levels for optimizing coupling for the fast ignitor ICF scheme.

This work was performed under the auspices of the U.S. Department of Energy by Lawrence Livermore National Laboratory under Contract DE-AC52-07NA27344. T. M. would like to acknowledge the assistance of D. Hey, C. Murphy, B. Westover, T. Yabuuchi, K. U. Akli, R. R. Freeman, G. E. Kemp, A. G. Krygier, L. D. Van Woerkom, R. Fedosejevs, H. Friesen, Y. Y. Tsui, S. D. Baton, M. Koenig, F. Perez, D. Turnbull, D. Price, and R. Combs with performing the experiment.

[1] M. Tabak, J. Hammer, M. E. Glinsky, W. L. Kruer, S. C. Wilks, J. Woodworth, E. M. Campbell, M. D. Perry, and R. J. Mason, Phys. Plasmas **1**, 1626 (1994).
[2] M. H. Key, Phys. Plasmas **14**, 055502 (2007).
[3] S. D. Baton *et al.*, Phys. Plasmas **15**, 042706 (2008).
[4] L. D. Van Woerkom *et al.*, Phys. Plasmas **15**, 056304 (2008).
[5] A. G. MacPhee *et al.*, Phys. Rev. Lett. **104**, 055002 (2010).
[6] J. A. King *et al.*, Phys. Plasmas **16**, 020701 (2009).
[7] S. Atzeni, Phys. Plasmas **6**, 3316 (1999).
[8] T. Ma *et al.*, Phys. Plasmas **16**, 112702 (2009).
[9] J. A. Koch *et al.*, Rev. Sci. Instrum. **74**, 2130 (2003).
[10] A. Pak, G. Gregori, J. Knight, K. Campbell, D. F. Price, B. Hammel, O. L. Landen, and S. H. Glenzer, Rev. Sci. Instrum. **75**, 3747 (2004).
[11] K. U. Akli *et al.*, Phys. Plasmas **14**, 023102 (2007).
[12] D. Welch, D. Rose, B. Oliver, and R. Clark, Nucl. Instrum. Methods Phys. Res., Sect. A **464**, 134 (2001).
[13] Y. T. Lee and R. M. More, Phys. Fluids **27**, 1273 (1984).
[14] M. Desjarlais, Contrib. Plasma Phys. **41**, 267 (2001).
[15] S. Atzeni, A. Schiavi, and J. R. Davies, Plasma Phys. Controlled Fusion **51**, 015016 (2009).
[16] J. MacFarlane, I. Golovkin, and P. Woodruff, J. Quant. Spectrosc. Radiat. Transfer **99**, 381 (2006).
[17] C. Hombourger, J. Phys. B **31**, 3693 (1998).
[18] J. Halbleib, R. Kensek, G. Valdez, S. Seltzer, and M. Berger, *Nuclear Science Symposium and Medical Imaging Conference, 1991* (IEEE, Bellingham, WA, 1991), Vol. 2, p. 1036.
[19] M. Roth, JINST **6**, R09001 (2011).
[20] T. Tanimoto *et al.*, Phys. Plasmas **16**, 062703 (2009).
[21] A. Link, R. R. Freeman, D. W. Schumacher, and L. D. V. Woerkom, Phys. Plasmas **18**, 053107 (2011).
[22] J. S. Green *et al.*, Nature Phys. **3**, 853 (2007).
[23] M. M. Marinak, G. D. Kerbel, N. A. Gentile, O. Jones, D. Munro, S. Pollaine, T. R. Dittrich, and S. W. Haan, Phys. Plasmas **8**, 2275 (2001).
[24] A. J. Kemp, B. I. Cohen, and L. Divol, Phys. Plasmas **17**, 056702 (2010).